MRS Communications (2023) 13:27–33
The Author(s) 2022
https://doi.org/10.1557/s43579-022-00307-0

MRS Communications

Research Letter

Conformational effect of Pt_2Ru_3 nanoparticle on surface coverage of CO/H_2 by materials informatics-integrated computational method

Md. Khorshed Alam, Department of Physics, University of Barisal, Barisal, Kornokathi 8200, Bangladesh
Shuhei Saito, Fumiya Hirosawa, Masaya Miyagawa, and Hiromitsu Takaba, Department of Environmental Chemistry & Chemical Engineering, School of Advanced Engineering, Kogakuin University, 2665-1 Nakano, Hachioji, Tokyo 192-0015, Japan

Address all correspondence to Hiromitsu Takaba at **takaba@cc.kogakuin.ac.jp**

(Received 18 August 2022; accepted 7 November 2022; published online: 30 November 2022)

Abstract

We investigated CO coverage (Θ_{CO}) on Pt_2Ru_3 nanoparticle with various morphologies in H_2/CO mixture gas atmosphere at 333 K by grand canonical ensemble Monte Carlo (GCMC) combined with quantitative structure–property relationship. In nanoparticles enclosed by (111) facets, Θ_{CO} was significantly reduced when the surface and the subsurface were composed of Pt and Ru, respectively. The nanoparticles with homogeneously mixed surface showed low Θ_{CO}, while the Janus-type showed high Θ_{CO}. A similar tendency was obtained in the (100)-enclosed nanoparticle. These results revealed that the homogeneous mixing of Pt and Ru on the surface is essential to increase the CO tolerance.

Introduction

Polymer electrolyte fuel cells (PEFCs) have been a promising device due to their high-power density and low operating temperature around 350 K. Pt and Pt-based materials have been known as a representative metal catalyst for an anode material when H_2 is used as the fuel.[1,2] One of the most fatal and ongoing problems is CO poisoning on the Pt surface: H_2 adsorption is considerably inhibited in the presence of CO, which is contained as an impurity in the H_2 fuel.[3,4] Because the H_2 gas is generally produced from hydrocarbons and alcohols, complete removal of CO at ppm level has extremely been difficult,[5] while it has been reported that even 10 ppm or less of CO is harmful to the cell performance.[6,7] Thus, the development of CO-tolerant electrocatalyst has been necessary, where the catalytic activity is maintained and precious Pt is also less used.

Solving the above problems, Pt-containing alloy metal nanoparticle has been explored.[8–10] Among various metal alloys, PtRu nanoparticle has been widely studied due to the high catalytic activity in the electrochemical oxidation of CO,[9,11–17] and Pt_2Ru_3 has been known as one of the most promising compositional formulae.[18–21] The synergistic effect of the alloying has been investigated focusing on the surface composition of the nanoparticle. Experimental studies have revealed that mixing of Pt and Ru is preferable for the efficient oxidation of CO on the Pt site by OH on the Ru site. Significance in Pt-rich surface has also been proposed to suppress the coverage of CO on the Ru site. Nevertheless, the ideal conformation of the PtRu nanoparticle has yet been uncovered due to difficulties in precise synthesis at sub-nm accuracy and atomic-level characterization of the nanoparticle surface.

Computational approaches such as quantum chemical calculation and molecular dynamics calculation have become significant since the late twentieth century. Because nanostructure and its physicochemical property are easily modeled and obtained by the computational approaches, the quantitative structure–property relationship (QSPR, hereafter) has gained attention as well as machine learning.[22–24] By the DFT method, the CO adsorption on the PtRu nanostructure has ever been investigated[25]: The adsorption energy of CO on the Ru site is larger than that on the Pt site, the latter of which is weakened by the alloying with Ru. We have previously reported the adsorption of CO, OH, and H on PtRu layers as a model of the nanoparticle surface, and found that the atop site is energetically more preferred in the CO adsorption than the bride and the hollow sites by the DFT method.[26] We have further applied Monte Carlo (MC) simulations to investigate conformational stability of homogeneously mixed polyhedron PtRu nanoparticle in the absence and presence of the adsorbates.[27,28] However, the effect of the morphologies including the surface composition and crystal facets has yet been unveiled, which are supposed to be significant in CO poisoning. In the present study, we investigated the adsorption behavior of CO and H_2 on the PtRu nanoparticles with various conformations by the grand canonical ensemble MC (GCMC)[29] with the aid of QSPR. It was found that homogeneous distribution of the Ru atoms in the surface is effective to minimize the CO coverage, and the most stable (111) facet is preferable. Under this condition, the CO coverage did not show strong dependency on the diameter of the nanoparticle.

Computational method

Outline

It is time consuming to calculate the interatomic energy of the whole system composed of the PtRu nanoparticle and

the adsorbates by using ab initio calculation. Hence, we used GCMC to determine whether the system was reached to equilibrium adsorption state, where changes in the adsorption energy were estimated by QSPR in which a multiple linear regression (MLR) was conducted by using structural descriptors of nanoparticles.

Calculations of adsorption energy

The adsorption energies of CO and H_2 on PtRu alloy surfaces were determined by DFT.[30–32] The detailed calculation condition and models for DFT calculations have been described in our previous papers.[26–28] Here, our DFT calculation is explained briefly. Slab models of five-layered PtRu alloy nanostructure were prepared, and some Pt atoms in the fcc structure are replaced with Ru atoms so that the compositional formula is Pt_2Ru_3. It has been reported that the fcc structure of Pt is maintained by the replacement when the Ru fraction is up to about 0.7.[33] After modeling the nanostructures, two molecules, CO and H_2, were set on the top layer. Their adsorption structure was energetically optimized by the DFT calculation.[34] This paper considered only the coadsorption structure for CO and H_2 because the surface is almost covered with H or CO in the following GCMC condition. Various conformations, some of which are shown in Fig. S1 were considered to calculate the coadsorption energy of CO and H_2.[28] According to previous studies, it was assumed that both CO and H_2 are adsorbed on the Pt or Ru atom because adsorption energy on the atop site is larger than that of the bridge and hollow sites.[26,35,36]

QSPR analysis

QSPR analysis was conducted to investigate the correlation between structural information of the PtRu nanostructure and the adsorption energy of H_2, CO, and H. In the used MLR, the general equation is as follows:

$$Y = b_1x_1 + b_2x_2 + \cdots + b_px_p, \quad (1)$$

where Y, b_n, and x_n ($n = 1, 2 \cdots p$) represent the adsorption energy, the regression coefficient, and the descriptor, respectively. The value of b_n is determined by the MLR analysis, while that of Y is derived from the DFT calculation (Y_{DFT}). The number of the atom or bond is used as the descriptor x_n. For example, $x_{Pt–CO}$ denotes the number of the Pt–CO bond. In contrast, $x_{Pt@S}$ denotes the number of the Pt atom composing the top layer. Metallic bonding is also considered based on the layers. When the bonding consists of two Pt atoms in the same layer, the descriptor is denoted as $x_{Pt–Pt}$, while it is denoted as x_{Pt_Pt} in the case of the different layers. By using b_n in the Eq. (1), the value of Y is calculated (Y_{EST}) and compared with Y_{DFT} to investigate validity of the model. Validity of the descriptors in the MLR has been discussed in our previous study.[28]

GCMC simulations of PtRu nanoparticle

Polyhedron-shaped PtRu nanoparticle enclosed mainly by the (111) or (100) facets was prepared from the fcc crystal structure of Pt. The number of atoms in the nanoparticle was 309 and 923 in diameters of 2.0 and 3.0 nm, respectively. Similar to the five-layered nanostructure, various conformations were subject to the calculation, in which effect on the CO tolerance will be discussed individually. The composition formula of the nanoparticles was always Pt_2Ru_3.

The gas adsorption at 333 K was modeled by GCMC. The total energy in GCMC was estimated by Eq. (1). One GCMC step consists of a randomly selected trial from generation or displacement. The concentration of CO is 300 ppm, and the pressure of H_2 is 70 kPa (the molar ratio of CO to H_2 is 4.3×10^{-4}). The adsorption of H_2 on the vacant Pt or Ru site is accepted only when the adjacent site is also vacant because the H_2 molecule dissociates to two H· (denoted as H, hereafter) by the catalysis of Pt or Ru. Because the orientation of the adsorbates was not considered in the GCMC simulation, an entropic effect due to freedom of molecular orientation is not fully considered. Other detail of the calculation condition is described in our previous paper.[27] During the GCMC simulation, the Pt and Ru atoms' conformations are fixed to reveal their effect on the adsorption property. According to our previous study, the number of steps is 50,000,000, which is sufficient to reach an equilibrium state.[28]

After the GCMC simulation, CO coverage, θ_{CO} was defined as the ratio of the number of the CO-adsorbed Pt or Ru atoms over that of the surface atoms. The H coverage θ_H was also calculated in a similar way, where one H_2 molecule occupies two metal sites due to the dissociation of the molecule to the two H atoms by the catalysis of Pt or Ru.

Results and discussion

Model validation

Table S1 shows the values of b_n obtained by the MLR analysis. The value of $b_{Ru–CO}$ is considerably smaller than that of $b_{Pt–CO}$, suggesting that CO is preferentially adsorbed on the Ru site. Compared to this result, the values of $b_{Ru–H2}$ and $b_{Pt–H2}$ are negative but rather larger. Thus, it is implied that CO adsorbs on the PtRu nanoparticle surface more easily than H. The values of the other regression coefficients are smaller, indicating that those parameters do not affect Y substantially. These results are reasonable because the objective variable Y is the adsorption energy, which is supposed to be dependent firmly on the direct bonding parameters of $b_{Ru–CO}$, $b_{Pt–CO}$, $b_{Ru–H2}$, and $b_{Pt–H2}$. Fig. S2 shows plots of Y_{EST} against Y_{DFT}. A reasonable correlation is observed between them, indicating that the adsorption energy is expressed by the descriptors with satisfactory accuracy. In the following sections, the equilibrium state is determined by GCMC, in which the changes in the adsorption energies were derived from the descriptors.

Significance in surface and subsurface metals

By the 50,000,000 steps of the GCMC simulation, the surface is covered entirely with CO and H. In other words, all the

adsorption sites on the nanoparticle surface are occupied under this condition. Based on this fact, θ_{CO} and θ_{H} were investigated in the polyhedron-shaped nanoparticles with various conformations, where the surface and the subsurface are composed of the different metals. For example, the nanoparticle with the Pt surface and the Ru subsurface are denoted as Pt/Ru. Pure Pt and Ru nanoparticles were also investigated individually. Figure 1 illustrates the pure Pt, pure Ru, Pt/Ru, and Ru/Pt nanoparticles. In all the nanoparticles, the surface is mainly enclosed by the (111) facets. The effect of the crystal facet will be discussed later. In the 2.0-nm Pt/Ru nanoparticle shown in Fig. 1(c), some Ru atoms are exposed on the surface due to a large specific surface area, while all the Ru atoms are fully covered with the Pt atoms in the 3.0-nm nanoparticle shown in Fig. 1(c'). In contrast to the Pt/Ru nanoparticle, all the Pt atoms in the subsurface are covered with the Ru atoms both in the 2.0- and 3.0-nm Ru/Pt nanoparticles shown in Fig. 1(d) and (d') due to the sufficient number of the Ru atoms.

Figure 2(A) shows θ_{CO} and θ_{H} in the PtRu nanoparticles illustrated in Fig. 1. In general, θ_{CO} gets higher in the larger diameter. For example, θ_{CO} is 30% and 59% in the 2.0-nm pure Pt and Ru nanoparticles, respectively, which increases to 53% and 73% when the diameter is 3.0 nm. This tendency is rationalized by b_n: Because the values of b_{Pt-CO} and b_{Ru-CO} are smaller than those of b_{Pt-H2} and b_{Ru-H2}, respectively, more stabilization energy is obtained by the adsorption of CO than H_2, resulting in the higher θ_{CO} in the larger nanoparticle with more surface atoms. Similarly, θ_{CO} is higher in the pure Ru nanoparticle than the pure Pt nanoparticle because b_{Ru-CO} is smaller than b_{Pt-CO}. This result is consistent with the fact that CO is adsorbed more strongly on the Ru site than the Pt site.[25]

The effect of the subsurface on θ_{CO} and θ_{H} was further investigated in the Pt/Ru and Ru/Pt nanoparticles. On the one hand, the 2.0-nm Pt/Ru nanoparticle, as illustrated in Fig. 1(c) shows the low θ_{CO}, 6.3%. This result is consistent with that of our previous study, where the adsorption energy of CO on the five-layered Pt_2Ru_3 nanostructure is considerably small when the surface and the subsurface consist of the pure Pt and Ru, respectively[26] as well as experimental studies.[9,18,19] Thus, the Ru atoms in the subsurface are found to be significant in the high CO tolerance. In contrast to the other nanoparticles, θ_{CO} in the Pt/Ru nanoparticle decreases to 3.3% in the case of 3.0 nm probably because the Ru atoms are entirely covered with the Pt atoms, as shown in Fig. 1(c'). On the other hand, θ_{CO} in the 2.0-nm Ru/Pt nanoparticle is 41%. This value is comparable to those of the pure Pt and Ru nanoparticles, and much higher than that in the Pt/Ru nanoparticle. The relatively high θ_{CO} originates from the strong adsorption of CO on the Ru site, which is in

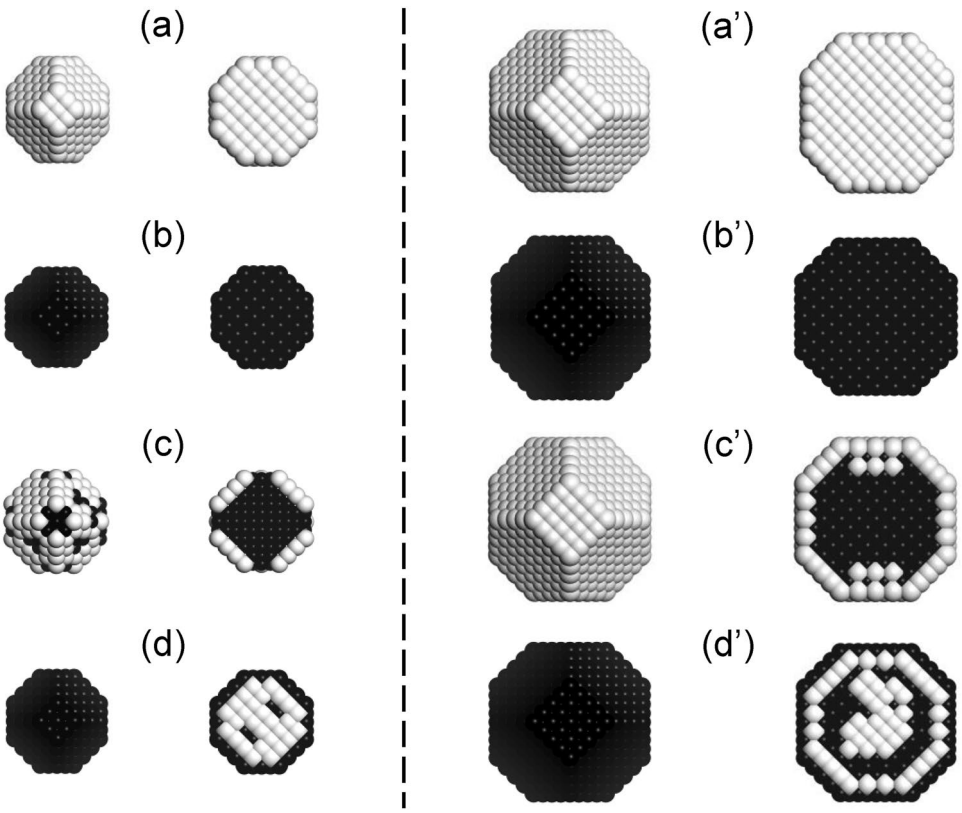

Figure 1. Illustration of (a) and (a') pure Pt, (b) and (b') pure Ru, (c) and (c') Pt/Ru, and (d) and (d') Ru/Pt nanoparticle, respectively. The forehead and the cross section of the nanoparticle are illustrated in the left and right halves in each panel, respectively. Diameters of (a–d) and (a'–d') are 2.0 and 3.0 nm, respectively. The polyhedron-shaped nanoparticles are mainly enclosed by the (111) facets.

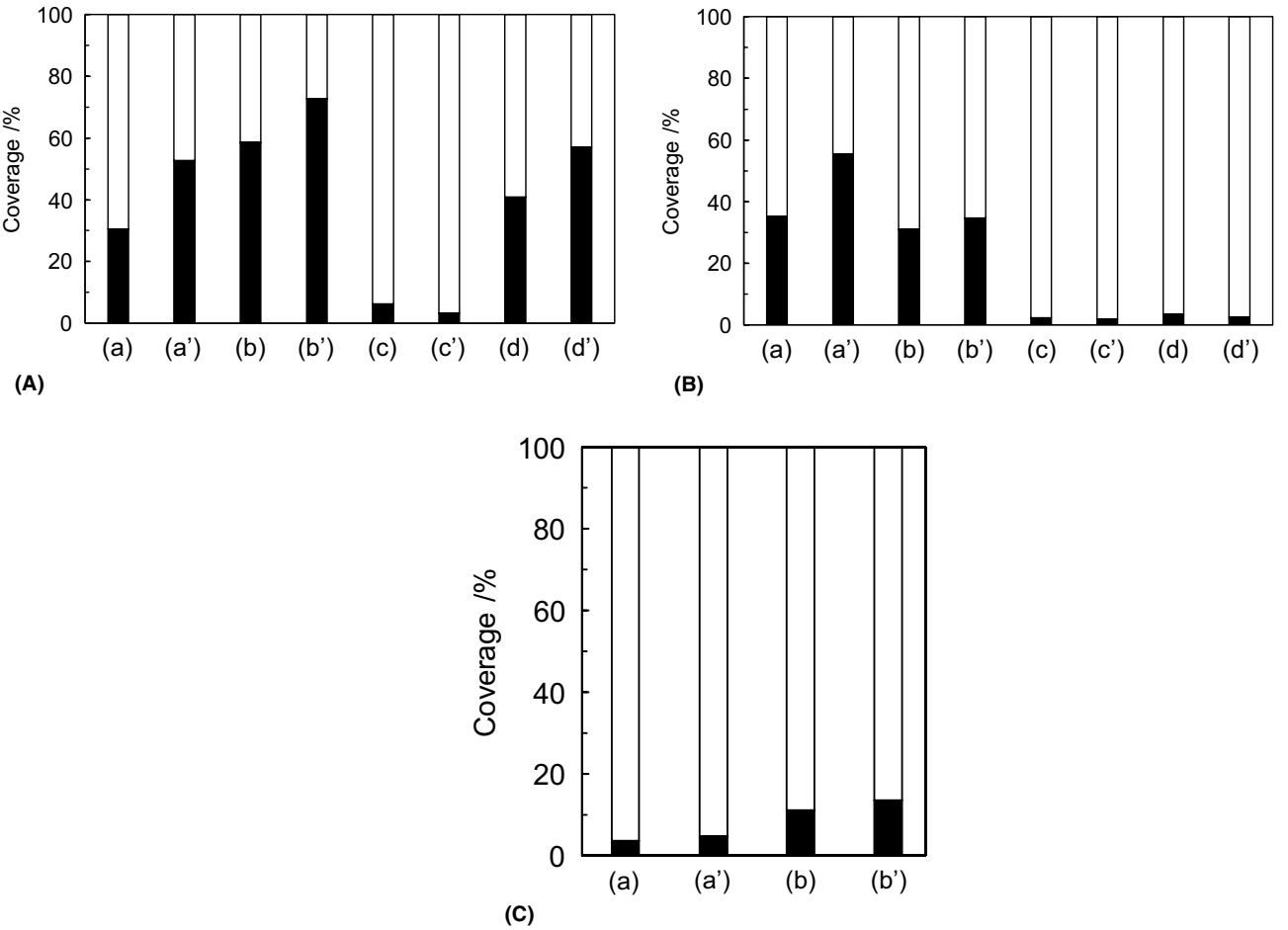

Figure 2. Coverage of CO (black) and H (white) in the nanoparticle with the various composition. The marks (a–d) and (a'–d') in panels A–C correspond to those in Figs. 1, 3 and 4, respectively.

harmony with the increase to 57% in the 3.0-nm nanoparticle with more Ru sites in the surface. Thus, θ_{CO} is found to be strongly affected by the elemental composition in the surface and the subsurface, both of which consist of a single metal, respectively.

Bimetallic nanoparticle surface for better CO tolerance

While the subsurface is found to play a considerable role in the CO tolerance, the surface composition should also be significant due to direct interaction with the adsorbates. Hence, the effect of the surface was further investigated in the PtRu nanoparticle with bimetallic surface. Figure 3 illustrates the nanoparticles with the different conformations, where the surface is mainly enclosed by the (111) facets. Hereafter, the nanoparticle composed of two different metal hemispheres (so-called Janus nanoparticle) is denoted as Pt·Ru. The well-mixed alloyed nanoparticle is simply denoted as PtRu. Focusing on the difference in subsurface, the nanoparticles illustrated in Fig. 3(a) and (b) are denoted as Pt·Ru/Pt·Ru and Pt·Ru/PtRu, respectively. Similarly, those shown in Fig. 3(c) and (d) are denoted as PtRu/Pt·Ru and PtRu/PtRu, respectively.

Figure 2(B) shows θ_{CO} and θ_{H} in the PtRu nanoparticles with the various conformations illustrated in Fig. 3. In the 2.0-nm Pt·Ru/Pt·Ru and Pt·Ru/PtRu nanoparticles, θ_{CO} is 35% and 31%, respectively, which is much higher than that in the Pt/Ru nanoparticle, 6.3% and relatively closed to the pure Pt nanoparticle, as shown in Fig. 2(A). In addition, θ_{CO} is 55% and 35% in the 3.0-nm Pt·Ru and Pt·Ru/PtRu nanoparticles, respectively, due to the increase in the Ru sites in the surface, which was already discussed in the previous section. Summarizing the above results, it is suggested that segregation of the Ru atoms in the nanoparticle surface is avoided to minimize θ_{CO}.

Considering that the 2.0-nm Pt/Ru nanoparticle shows the low θ_{CO} in spite of the partial exposure of the Ru atoms in the surface shown in Fig. 1(c), mixing of Pt and Ru in the surface seems significant. Indeed, θ_{CO} is only 2.3% and 3.4% in the PtRu/Pt·Ru and PtRu/PtRu nanoparticle, respectively, when the diameter is 2.0 nm. Because both values are lower than

that in the Pt/Ru nanoparticle, 6.3% shown in Fig. 2[A(c)], it is found that the homogeneous mixing of Pt and Ru in the surface endows the nanoparticle with the superior CO tolerance. This result is consistent with that in the experimental study, where random distribution of Pt and Ru is claimed to be significant.[20] The diameter dependency of θ_{CO} is also noteworthy: θ_{CO} is slightly decreased to 1.9% and 2.5% in the 3.0-nm PtRu/Pt·Ru and PtRu/PtRu nanoparticles, respectively. From a viewpoint of nanoparticle synthesis, our result is beneficial: controlling the diameter in the order of 0.1 nm is not strongly required to achieve the high CO tolerance. In addition, theoretical studies previously reveal that the bimetallic surface is energetically stable in the Pt_2Ru_3 nanoparticle.[27,28] Therefore, it is concluded that the homogeneous mixing of the Pt and Ru atoms in nanoparticle surface is considerably effective to minimize θ_{CO}.

Effect of crystal facets

It is true that the (111) facets are the most stable and predominant in the Pt skeleton with the fcc structure, but the (100) facets should be paid attention because of the second most stable crystal facets. In single-metal nanoparticle, it is reported that nanocube enclosed by the (100) facets often shows higher catalytic activities than the spherical nanoparticle enclosed mainly by the (111) facets due to high surface energy.[37,38] Hence, the polyhedron-shaped nanoparticle predominantly enclosed by the (100) facets was investigated. Figure 4 illustrates the PtRu/Pt·Ru and PtRu/PtRu nanoparticles with the large (100) facets in the diameter of 2.0 and 3.0 nm. Figure 2(C) shows θ_{CO} and θ_{H} of the corresponding nanostructures. In the 2.0-nm PtRu/Pt·Ru and PtRu/PtRu nanoparticles, θ_{CO} is 3.7% and 11%, respectively. The both values are higher than those in the nanoparticles enclosed by the (111) facets. This result is consistent with that reported previously, where the (111) facets show the superior CO tolerance compared to the (100) facets in electrocatalytic methanol oxidation.[39] It is true that utility as the catalyst is strongly dependent on the reaction, but our result demonstrates that the morphology including the shape suitable for the low θ_{CO} would be predictable by the combination of the QSPR analysis and the GCMC simulation. The similar tendency is also observed in the 3.0-nm nanoparticle: θ_{CO} is 4.7% and 14% in the PtRu/Pt·Ru and PtRu/PtRu nanoparticles, respectively. Thus, it is found that the (111) facets are more preferable than the (100) facets on the issue of the CO coverage, the former of which is generally exposed predominantly in the PtRu nanoparticle.

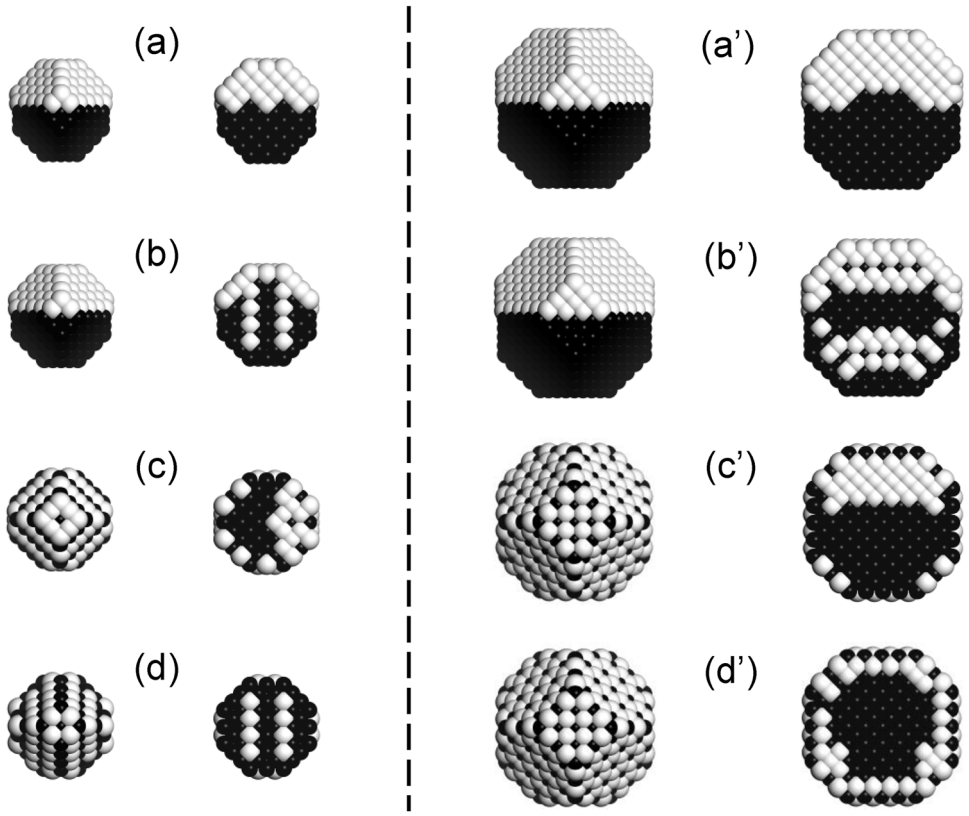

Figure 3. Illustration of (a) and (a') Pt·Ru/Pt·Ru, (b) and (b') Pt·Ru/PtRu, (c) and (c') PtRu/Pt·Ru, and (d) and (d') PtRu/PtRu nanoparticle, respectively. The forehead and the cross section of the nanoparticle are illustrated in the left and right halves in each panel, respectively. Diameters of (a–d) and (a'–d') are 2.0 and 3.0 nm, respectively. The polyhedron-shaped nanoparticles are mainly enclosed by the (111) facets.

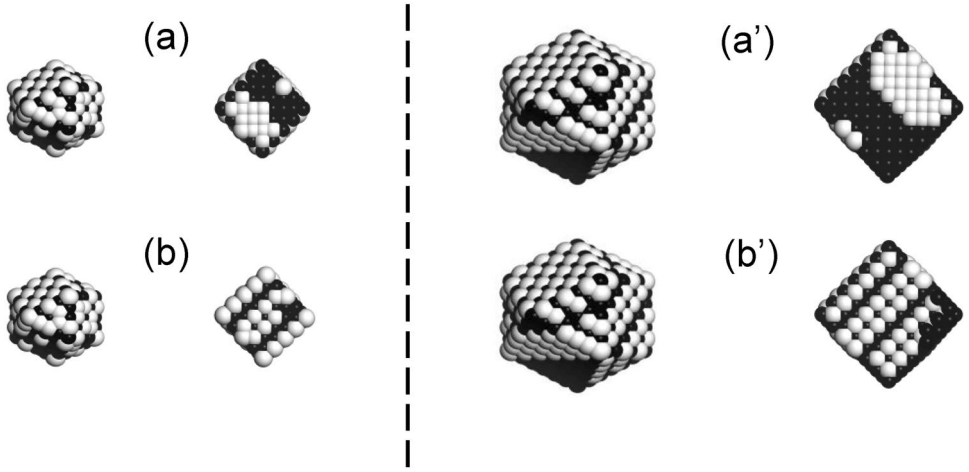

Figure 4. Illustration of (a) and (a') PtRu/Pt·Ru, and (b) and (b') PtRu/PtRu nanoparticle, respectively. The forehead and the cross section of the nanoparticle are illustrated in the left and right halves in each panel, respectively. Diameters of (a) and (b), and (a') and (b') are 2.0 and 3.0 nm, respectively. The polyhedron-shaped nanoparticles are mainly enclosed by the (100) facets.

Conclusion

In the present study, we investigated ideal morphology of the Pt_2Ru_3 nanoparticle to show low θ_{CO} by using the GCMC simulation combined with the QSPR analysis. The adsorption energy obtained by the DFT calculation was well explained by using the number of atoms and bonds as the descriptors, indicating that the equilibrium state is determined by the structural information. It was found that Pt_2Ru_3 nanoparticle basically shows low θ_{CO} compared to pure metal Pt and Ru nanoparticles. Specifically, the nanoparticle composed of Pt surface and Ru subsurface shows superior CO tolerance. Effect of mixing of the two metals in the surface was found to be noticeable: θ_{CO} is < 5% in the diameter of 2.0 nm, and ca. 10% even in 3.0 nm, which is also independent of the crystal facet. Therefore, it was concluded that controlling the mixing state rather than the diameter and crystal facet is effective to develop superior CO-tolerant Pt_2Ru_3 nanoparticle.

Author contributions

MKA, SS, and FM: performed the whole calculation and data analysis. MM: also conducted data analysis and wrote the manuscript. HT: supervised the whole project. All authors approved the final version of the manuscript.

Funding

We are grateful to the New Energy and Industrial Technology Development Organization (NEDO) for providing partially financial support.

Data availability

The datasets generated during and/or analyzed during the current study are available from the corresponding author on reasonable request.

Declarations

Conflict of interest

We declare no conflict of interests.

Open Access

Supplementary Information

The online version contains supplementary material available at https://doi.org/10.1557/s43579-022-00307-0.

References

1. Z. Song, M.N. Banis, H. Liu, L. Zhang, Y. Zhao, J. Li, K. Doyle-Davis, R. Li, S. Knights, S. Ye, G.A. Botton, P. He, X. Sun, ACS Catal. **9**, 5365 (2019)
2. T. Kim, Y. Kwon, S. Kwon, J.G. Seo, ACS Omega **5**, 26902 (2020)
3. R.A. Lemons, J. Power Sources **29**, 251 (1990)
4. T.R. Ralph, M.P. Hogarth, Platin. Met. Rev. **46**, 117 (2002)
5. O. Korotkikh, R. Farrauto, Catal. Today **62**, 249 (2000)
6. K.K. Bhatia, C.-Y. Wang, Electrochim. Acta **49**, 2333 (2002)
7. A.A. Franco, M. Guinard, B. Barthe, O. Lemaire, Electrochim. Acta **54**, 5267 (2009)
8. G. Cabello, R.A. Davoglio, J.F. Marco, A. Cuesta, J. Electroanal. Chem. **870**, 114233 (2020)
9. H. Igarashi, T. Fujino, Y. Zhu, H. Uchida, M. Watanabe, Phys. Chem. Chem. Phys. **3**, 306 (2001)
10. S.M.M. Ehteshami, S.H. Chan, Electrochim. Acta **93**, 334 (2013)
11. H.A. Gasteiger, N. Markovic, P.N. Ross Jr., E.J. Cairns, J. Phys. Chem. **98**, 617 (1994)
12. S.R. Brankovic, N.S. Marinkovic, J.X. Wang, R.R. Adžić, J. Electroanal. Chem. **532**, 57 (2002)
13. P. Waszczuk, A. Wieckowski, P. Zelenay, S. Gottesfeld, C. Coutanceau, J.-M. Léger, C. Lamy, J. Electroanal. Chem. **511**, 55 (2001)
14. G. Roh, H. Lee, Y. Jeong, J.H. Kim, H. Kim, Int. J. Hydrogen Energy **44**, 21588 (2019)
15. M. Tian, S. Shi, Y. Shen, H. Yin, Electrochim. Acta **293**, 390 (2019)
16. J. Zhang, X. Qu, Y. Han, L. Shen, S. Yin, G. Li, Y. Jiang, Appl. Catal. B **263**, 118345 (2020)
17. M. González-Hernández, E. Antolini, J. Perez, Int. J. Hydrogen Energy **45**, 5276 (2020)
18. T. Sato, K. Kunimatsu, K. Okaya, H. Yano, M. Watanabe, H. Uchida, Energy Environ. Sci. **4**, 433 (2011)
19. T. Sato, K. Kunimatsu, K. Okaya, H. Yano, M. Watanabe, H. Uchida, ACS Catal. **2**, 450 (2012)
20. T. Takeguchi, T. Yamanaka, K. Asakura, E.N. Muhamad, K. Uosaki, W. Ueda, J. Am. Chem. Soc. **134**, 14508 (2012)
21. N. Narischat, T. Takeguchi, T. Mori, S. Iwamura, I. Ogino, S.R. Mukai, W. Ueda, Int. J. Hydrogen Energy **41**, 13697 (2016)
22. A. Balfourier, V. Mulens-Arias, F. Gazeau, F. Carn, J. Phys. Chem. C **124**, 8938 (2020)
23. S. Lotfi, S. Ahmadi, P. Kumar, RSC Adv. **11**, 33849 (2021)
24. Y. Jia, X. Hou, Z. Wang, X. Hu, ACS Sustain. Chem. Eng. **9**, 18 (2021)
25. Q. Ge, S. Desai, M. Neurock, K. Kourtakis, J. Phys. Chem. B **105**, 9533 (2001)
26. Md.K. Alam, S. Saito, H. Takaba, J. Mater. Res. **31**, 2617 (2016)
27. Md.K. Alam, S. Saito, H. Takaba, J. Mater. Res. **32**, 1573 (2017)
28. Md.K. Alam, H. Takaba, MRS Commun. **8**, 562 (2018)
29. N. Metropolis, A.W. Rosenbluth, M.N. Rosenbluth, A.N. Teller, E. Teller, J. Chem. Phys. **21**, 1087 (1953)
30. B. Delley, J. Chem. Phys. **92**, 508 (1990)
31. B. Delley, J. Phys. Chem. **100**, 6107 (1996)
32. B. Delley, J. Chem. Phys. **113**, 7756 (2000)
33. E. Antolini, Mater. Chem. Phys. **78**, 563 (2003)
34. W. Kohn, L. Sham, J. Phys. Rev. **140**, A1133 (1965)
35. H. Orita, N. Itoh, Y. Inada, Chem. Phys. Lett. **384**, 271 (2004)
36. M.T.M. Koper, T.E. Shubina, R.A. van Santen, J. Phys. Chem. B **106**, 686 (2002)
37. M. Jin, H. Zhang, Z. Xie, Y. Xia, Energy Environ. Sci. **5**, 6352 (2012)
38. P. Zhang, Y. Sui, G. Xiao, Y. Wang, C. Wang, B. Liu, G. Zou, B. Zou, J. Mater. Chem. A **1**, 1632 (2013)
39. L. Huang, X. Zhang, Q. Wang, Y. Han, Y. Fang, S. Dong, J. Am. Chem. Soc. **140**, 1142 (2018)